

Reconciling NMR Measurements and Numerical Simulations: Assessment of Temperature and Diffusive Coupling Effects on Two-Phase Carbonate Samples¹

E. Toumelin², C. Torres-Verdín², S. Chen³, and D. M. Fischer⁴

ABSTRACT

Nuclear Magnetic Resonance (NMR) is the only logging technique sensitive to pore-size distribution and pore structure. However, quantitative interpretation of NMR data can become uncertain in carbonate rocks because of unaccounted diffusion coupling between existing pore scales. The objective of this study is to assess the relative importance of diffusion coupling and temperature on NMR measurements performed on a few carbonate samples.

The core of our work is based on the analysis of experimental NMR measurements and on the use of numerical simulations. The numerical simulation algorithm consists of Monte-Carlo random walks in three dimensions and accounts for two-phase fluid saturations in the presence of a bimodal pore-size distribution. NMR coupling effects are modeled by including simple cross-interactions between the fluids within the different types of pores. We

present a method based on rock image analysis to calibrate the numerical model to NMR laboratory measurements acquired in complex carbonate rocks at two stages of fluid saturation. The derived simulation models are subsequently used to generate equivalent decoupled responses of the samples. Comparison of these decoupled responses with experimental data allows one to assess the effect of diffusion coupling. The experimental data were also used to quantify the temperature dependence of NMR measurements and movable fluid volumes, normally determined assuming either a constant a priori formation $T_{2\text{cutoff}}$, or else parameters derived at ambient temperature. Finally, an analysis is made of the sensitivity of conventional permeability models to the combined effects of temperature and diffusion coupling, as evidenced by the core samples considered in this paper.

INTRODUCTION

Pore structures of carbonate rocks are known to be much more difficult to quantify than those of sandstones. The genesis of carbonate rocks is commonly associated with both chemical and biological processes that can cause large variations of pore size, shape, texture, and degree of dissolution/cementation. Carbonate rocks also exhibit a large

degree of heterogeneity in the form of (a) partially isolated pores and (b) presence of both intra- and inter-granular pores. Petrographic or standard core analysis techniques often face serious technical difficulties in determining whether or not an existing “vug” is hydraulically isolated from the rest of the pore structure. Similarly, it is difficult to identify in the laboratory whether secondary, inter-

Manuscript received by the Editor October 21, 2002; revised manuscript received January 27, 2003.

¹Originally presented at the SPWLA 43rd Annual Logging Symposium, June 2–5, 2002, Oiso, Japan, Paper JJJ.

²The University of Texas at Austin, Austin, TX USA

³Baker Atlas, Houston, TX USA

⁴Baker Atlas Inteq, Celle, Germany

©2003 Society of Professional Well Log Analysts. All rights reserved.

connected micropores provide significant diffusive connectivity to the overall pore network. The detection and quantification of such structural properties and of their impact on pore connectivity and fluid transport is essential to the characterization of carbonate reservoir quality and producibility.

As the only logging technique currently available to characterize pore size distributions, Nuclear Magnetic Resonance (NMR) logging has been used to assess a handful of key petrophysical parameters, such as irreducible bulk volume (BVI), clay-bound water volume (CBW), movable bulk volume (BVM), effective (ϕ_e) and total porosity (ϕ_T), and permeability index (k). All of these parameters are related to the amount and the distribution of the fluids within the pore structure. Thus, an understanding of how NMR measurements respond to variations of pore structure is essential to quantify petrophysical formation properties.

Most of the currently available NMR interpretation models and parameters thereof, such as $T_{2\text{cutoff}}$, spectral BVI, CBW, and Timur-Coates permeability index, are based on the concept of pore-size distributions. This concept is most suitable in cases where a deterministic relationship exists between pore size and throat size. Although these models have been applied successfully to the interpretation of sandstones, and to some extent of carbonates, modifications are often required to accommodate local geological and petrophysical knowledge. Some modifications are empirical (Quintero et al., 1999; Allen et al., 2001), while others stem from more fundamental considerations (Ramakrishnan et al., 1999; Godefroy et al., 2001).

METHODOLOGY

Even though large variations are expected in the spatial distribution of pores in carbonates, it is important to quantify their effect on both petrophysical properties and log interpretation. The main thrust of this paper is to report a thorough analysis performed on a few carbonate samples of the dependence of NMR measurements on temperature and diffusion coupling. We carry out this analysis by using NMR measurements at different temperatures and numerical simulations that take into account diffusion coupling and temperature effects. This paper is organized as follows. First, we briefly describe the three main core samples used in our study with emphasis on their pore structure and their propensity to exhibit diffusion coupling. Subsequently, we describe the NMR experimental protocol used to obtain core measurements at different temperatures and fluid saturations. We then summarize the numerical algorithm used to model the NMR response in the presence of bimodal, micro-porous carbonate rocks. We show how both the NMR

measurements and the petrographic analysis can be synthesized into a parametric numerical model of bimodal porosity capable of describing the pore complexity exhibited by the core samples. The effect of temperature on NMR measurements is then investigated, and the comparison between numerical simulations and experimental measurements is extended to explore the role played by temperature in diffusive coupling. Lastly, cumulative porosity curves derived from both NMR experiments and numerical simulations are used to assess the BVI errors that come from using $T_{2\text{cutoff}}$ that are independent of temperature and diffusive coupling. We conclude by studying the stability of the conventional permeability models to the presence of temperature variations in the measured rocks, and the need to correct $T_{2\text{cutoff}}$ values in log analysis when neither temperature nor diffusion coupling are negligible.

PORE STRUCTURE OF THE SAMPLES

The three samples considered in this paper are compacted, micritized limestones retrieved from the same well but exhibiting different facies. Back Scattered Electron (BSE) imaging was used to analyze the pore structure of these samples (Prior et al., 1999) and to measure pore-size distributions and porosities, ϕ_{BSE} , for pores larger than 2 microns. Scattering Electron Microscope (SEM) was also used to provide high-resolution spatial images of the pore-matrix structure (Anselmetti et al., 1998). A complementary laboratory core-plug measurement was performed to assess total porosity ϕ_T , which in turn allowed the quantification of micro-porosity otherwise unaccounted by the BSE analysis, i.e., $\phi_{\text{micro}} = \phi_T - \phi_{\text{BSE}}$.

Pore geometry analysis helped to identify several pore types, or pore modes, within the samples, namely:

- Mode 1: Large primary inter-connected pores with average diameters larger than 60 μm . Pores exhibit variable cementation, thereby providing partial diffusion coupling with the surrounding micro-porosity region.
- Mode 2: Large secondary dissolution pores, with average diameters within the range of 20-60 μm . These pores are largely hydraulically isolated and hence remain uncoupled to other pore modes.
- Mode 3: These are pores developed between circum-granular cement crystals ranging in diameter from 5 to 15 μm . Due to their proximity to smaller micro-porosity regions, they can be regarded as coupled with the latter.
- Mode 4: These pores exhibit diameters of 0.5 μm or less and therefore constitute the micro-porosity associated with ϕ_{micro} . They are developed within the matrix and contain irreducible water.

Porosities and average radii of pore modes 1 through 3

**Reconciling NMR Measurements and Numerical Simulations:
Assessment of Temperature and Diffusive Coupling Effects on Two-Phase Carbonate Samples**

were quantified using the pore-size distribution estimated via BSE analysis. In terms of pore-size distributions, the main features of the samples are as follows:

- **Sample A** mostly exhibits a combination of small-size (modes 3 and 4) diffusively coupled porosities amounting to 13.6% of the bulk volume, with 10% vuggy (mode 2), isolated macro-porosity. An example of this pore structure is provided by the SEM images shown in Figure 1, where one can easily recognize abundant microporosity as well as a few isolated vugs. The high degree of diffusion coupling is likely, since the thin sections (Figure 2) show that most of the calcite-free micro-pore

space clearly imbibes epoxy. The measured permeability to water is low, equal to 4 mD.

- **Sample B** mainly consists of 8.1% primary macro-porosity (mode 1) partially coupled with 5.1% microporosity (mode 4), in addition to 5% isolated secondary macro-porosity (mode 2). As shown by the SEM images of Figure 3, this sample exhibits a dual porosity characterized by the remarkable structural organization of matrix grains into intrinsically micro-porous packs. The thin sections of Figure 4 show partial imbibition of epoxy into the intragranular micro-porosity. The measured permeability of sample B to water is 70 mD.
- **Sample C** exhibits the highest macro-porosity among the three samples reported in this section. The major part of

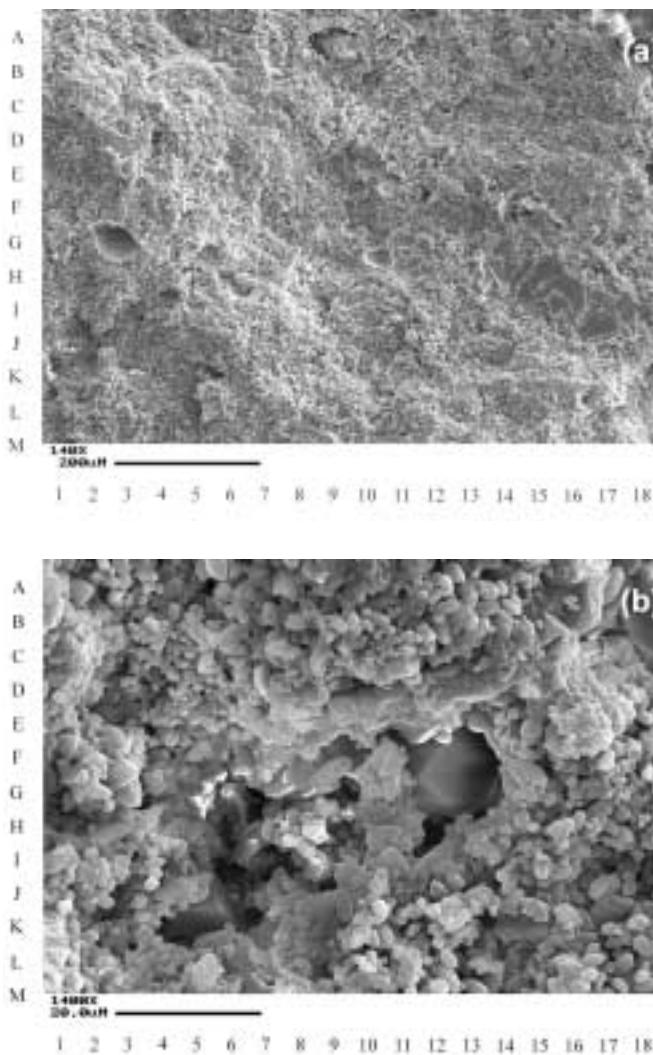


FIG. 1 SEM images of sample A at 140x (a) and 1400x (b) magnification. These pictures show the extensive micritization of the rock matrix and the isolation of scarce macro-pores. There is no appreciable amount of cement to prevent contact between intra- and intergranular pore spaces.

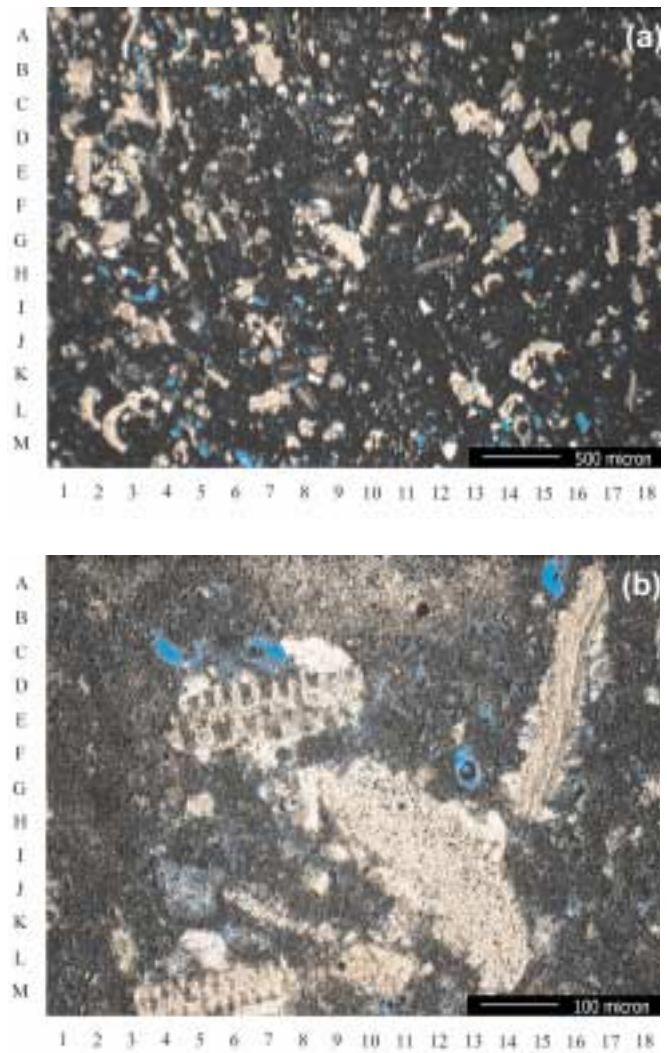


FIG. 2 Thin section images from sample A. Except for calcite-bearing areas (shown in white on the pictures), epoxy has been consistently imbibed by the micro-porous matrix.

the porosity is associated with primary macro-porosity regions of mode 1 (17% porosity), while the remaining 4% porosity is evenly distributed among the remaining three pore modes. The SEM images of Figure 5 show the structure of the macro-porosity and suggest good cementation along the macro-pore surfaces. This cementation explains the impermeability of the micro-porosity to epoxy (Figure 6). The highly connected macro-pore structure explains the relatively high value of the measured water permeability, equal to 980 mD.

As illustrated in Figure 7, the BSE-based pore-size distribution allowed us to identify pore modes 1 through 3. The

SEM images were then used to estimate the micro-pore size (mode 4) in the range of 0.2 to 0.5 μm .

NMR EXPERIMENTS

Nuclear magnetic resonance measurements of the three core samples were performed with a MARAN ULTRA system operating at a frequency of 2.3 MHz. The samples were first measured with 100% water saturation ($S_w = 1$) at different temperatures between 4 and 65°C (4, 22, 45, and 65°C for samples A and C; 10, 22, 45, and 60°C for sample B).

Subsequently, the same samples were desaturated to their irreducible water saturation (S_{wir}) state by centrifugation. The pressure applied to the samples during centrifugation was equal to 60 psi (414 kPa) during 24 hours or more.

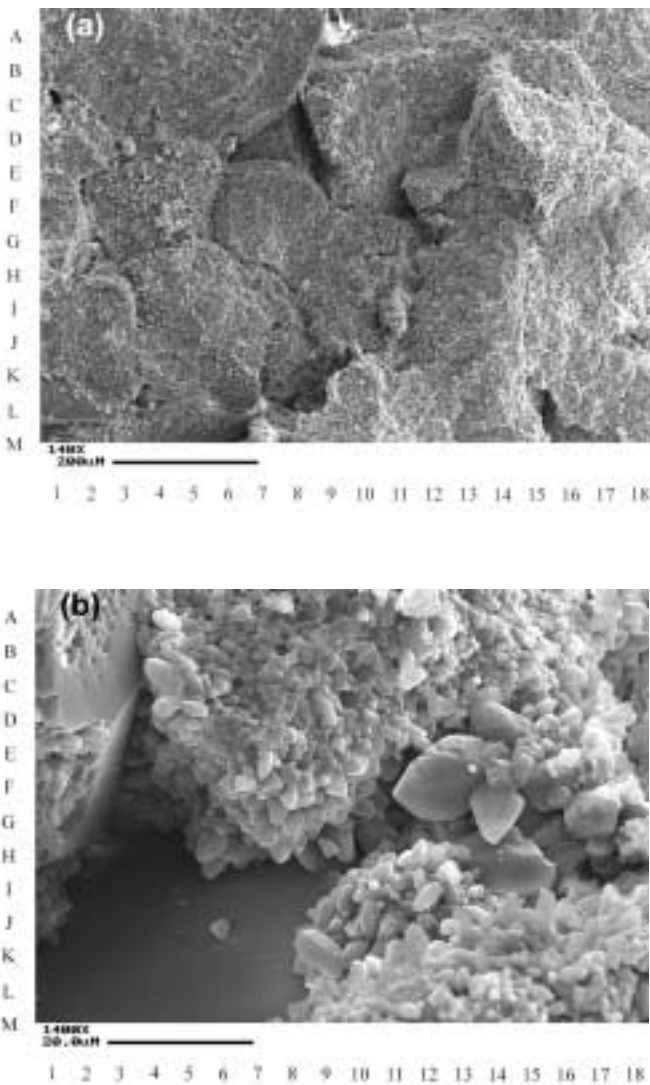


FIG. 3 SEM images of sample B at 140x (a) and 1400x (b) magnification. Macro-porosity and general agglomeration of grains into packs are well defined in the images. The images also indicate the presence of cementation crystals at the limit of some micritized grain packs (macro-pore surface).

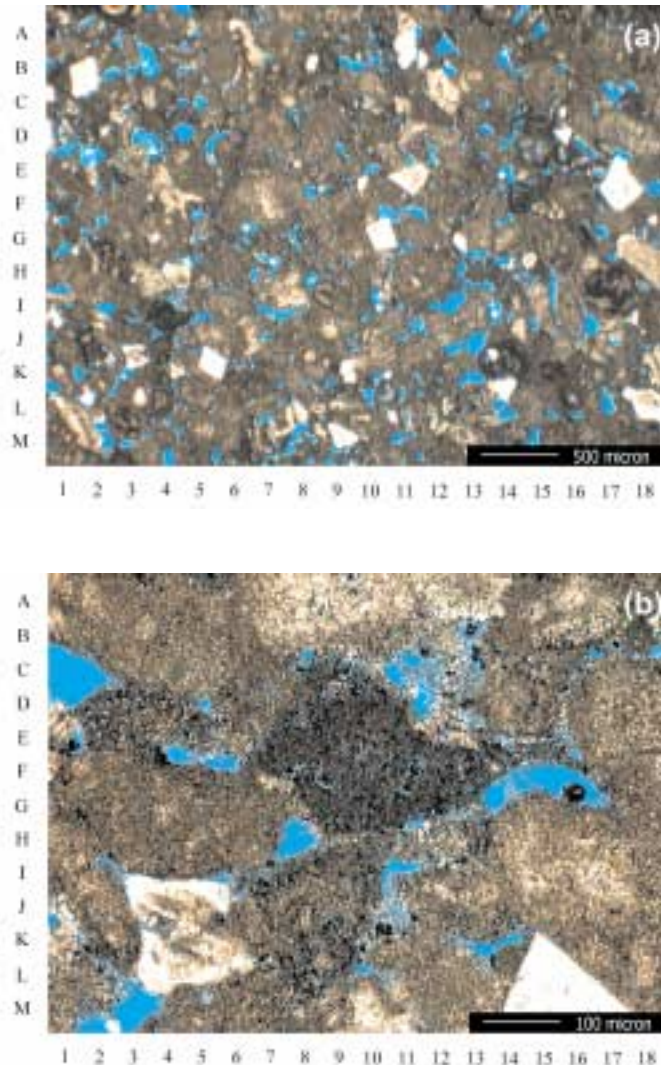


FIG. 4 Thin sections from sample B exhibiting partial epoxy imbibition by the micro-porous regions.

**Reconciling NMR Measurements and Numerical Simulations:
Assessment of Temperature and Diffusive Coupling Effects on Two-Phase Carbonate Samples**

Moreover, it was assumed that all moveable water had been removed when the measured expelled water volume was observed to be stable for 8 hours. All NMR measurements for the irreducible water saturated samples were acquired at regulated room temperature (22°C).

A CPMG sequence was used to obtain echo trains of up to 5000 echoes with even time spacing, TE , of 1 ms and in the absence of a magnetic field gradient. Measurements were repeated and stacked to ensure signal-to-noise ratios greater than 100. We made use of a discrete, multi-exponential relaxation model with a sufficiently wide T_2 bin

range to invert the echo trains into transverse relaxation (T_2) distributions. The inversion technique employs a curvature-smoothing regularization (Chen et al., 1999) to stabilize the solutions in the presence of noise. Figure 8 shows the T_2 distributions obtained from NMR measurements performed at $S_w = 1$ and S_{wir} for each of the three core samples.

NMR SIMULATION MODEL

The algorithm used to simulate numerically the NMR response of fluid-filled carbonate rocks replicates a conditional Monte Carlo random-walk procedure. Conceptually, the diffusive coupling model and the dual random-walk algorithm are a generalization of the algorithm reported by

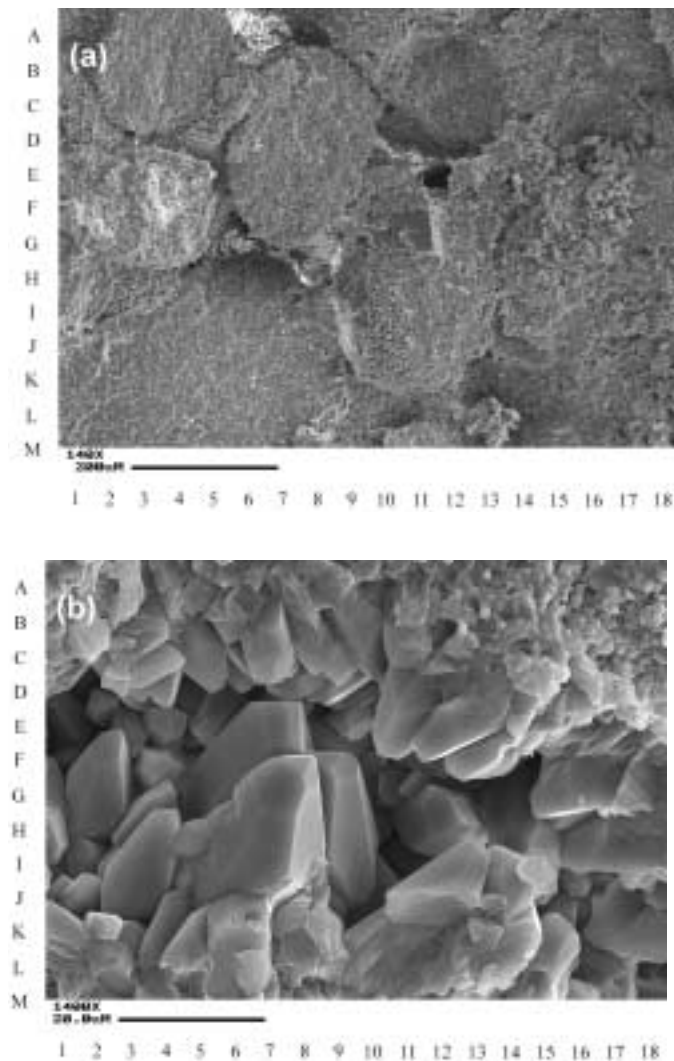


FIG. 5 SEM images of sample C at 140x (a) and 1400x (b) magnification. The structure in panel (a) has the same appearance as that of sample B, although the BSE analysis shows that large pores are more numerous in sample C. The high density of calcite crystals provides strong cementation of the macro-pores.

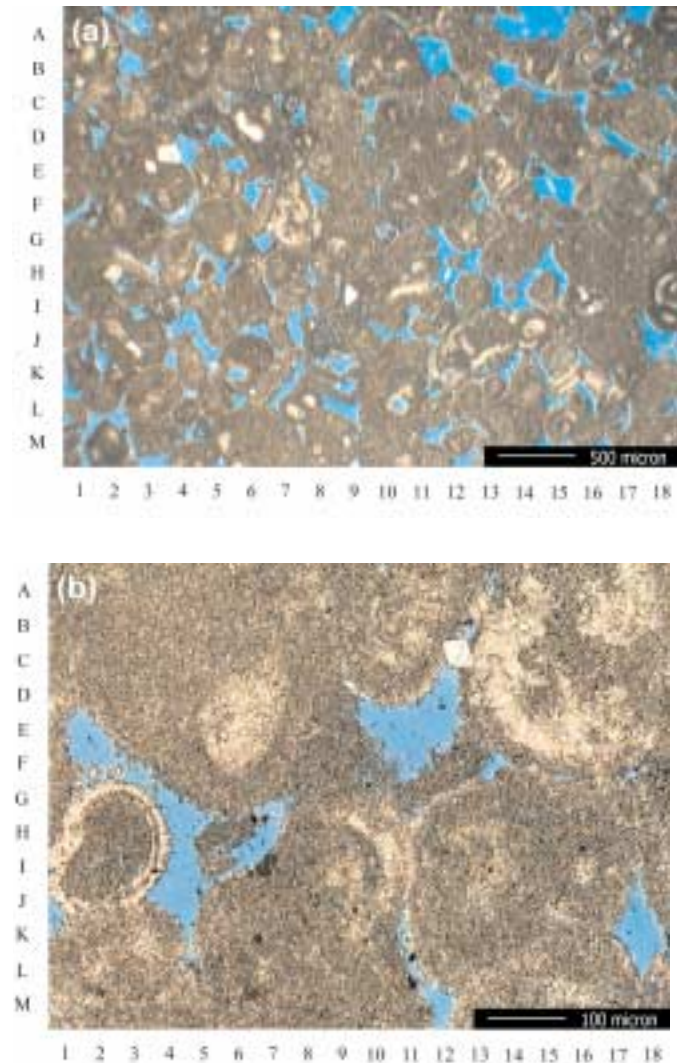


FIG. 6 Thin sections from sample C showing no imbibition of epoxy outside the macro-porous regions.

Ramakrishnan et al. (1999). However, instead of modeling the NMR response as a histogram of walked times, our algorithm simulates the CPMG echo decay in the time domain. This approach requires tracking of the NMR signal phase evolution resulting from both the random walk and the assumed NMR pulse sequence.

Model geometry

The simulation model was constructed with a three-dimensional (3D) bimodal pack of spheres intended to replicate the pore-structure geometry of carbonate formations, in which micro-grains are arranged into packs. As in the example of Figure 3, the simulation model accounts for intra-granular porosity regions that constitute the grain packs, while different types of inter-granular porosity (characterized by different pore sizes and degrees of cementation, depending on diagenesis) exist between the packs. The geometrical construction of the 3D model is based on the following assumptions:

- Bimodal pore-size distribution,
- Periodic geometry,
- Isotropic pores,

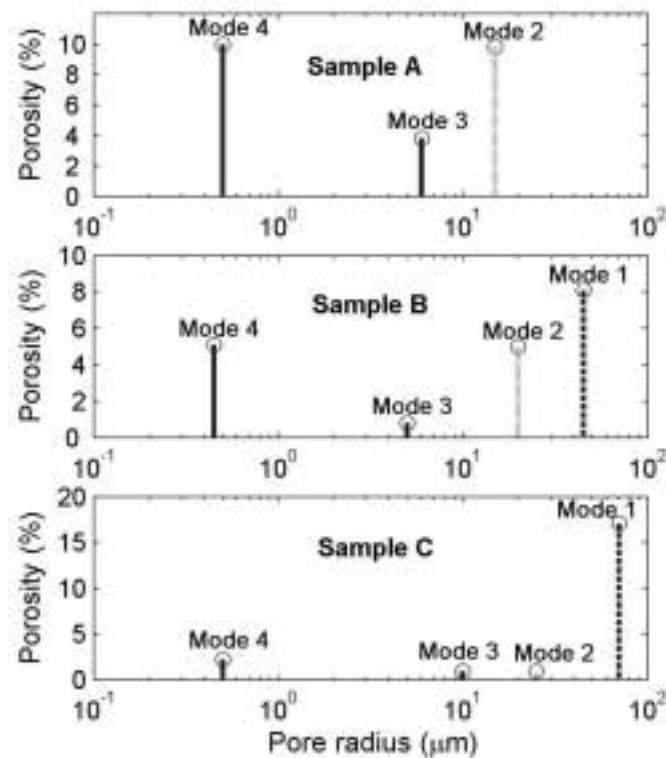


FIG. 7 Pore-size modes recognized in samples A, B and C. Plain stems correspond to coupled porosity modes, dash stems, to partially coupled primary porosity, and dot stems to a-priori uncoupled vuggy porosity.

- Spherical, compacted micro-grains, and
- Spherical, compacted grain packs.

At the micro- (macro-) scale, each grain (grain pack) is constructed with a sphere inscribed into a concentric cubic cell. If the sphere does not completely fill its cubic unit, then the complementary volume is considered filled with fluids. Furthermore, fixed blobs of gas centered on the macro-pore space can be included in the model to represent partial saturations of an immiscible non-wetting gas phase, while the micro-porosity can only be filled with wetting fluid. Figure 9 shows a 3D period of this bimodal pore-network structure. A wide variety of pore sizes can be modeled by adjusting the values of the grain (or grain pack) radii, and the sizes of the corresponding cubic cell.

Random-walk algorithm

At each iteration of the Monte Carlo simulation procedure, a fictitious proton is randomly chosen within the space formed by the available pore volume. This proton is then

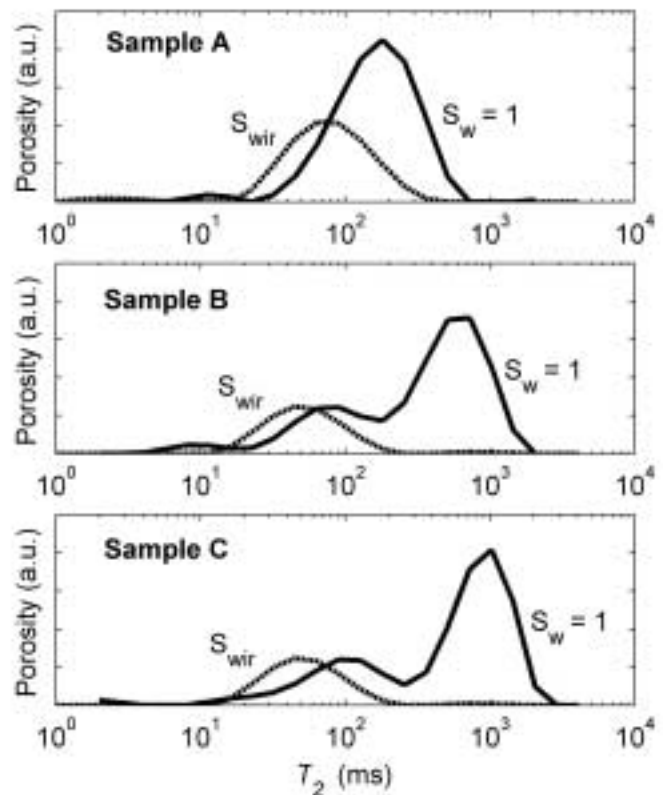


FIG. 8 T_2 distributions of NMR measurements performed at ambient temperature on samples A, B, and C. Dashed curves represent the measurements at irreducible water saturation. Solid curves represent measurements performed at 100% water saturation.

displaced to a new location dictated by a random-walk algorithm that operates according to two possible strategies. Depending on the proximity of the proton to the surface of material discontinuity (pore wall or fluid phase interface), either a conventional random-walk strategy or a First-Passage-Time technique (Zheng and Chiew, 1989) is implemented to displace the proton to its new location.

The First-Passage-Time strategy is based on the analytical solution of the unbounded diffusivity equation. This yields a stochastic relationship between the mean square displacement, R^2 , during each step, and its duration, Δt , with a maximum of probability close to the free space bulk diffusivity, i.e.,

$$D_o = \frac{\langle R^2 \rangle}{6\Delta t}. \quad (1)$$

In the above relationship, R is limited to the largest displacement allowed by the surrounding fluid boundaries, while Δt is constrained by the time sampling period TE corresponding to the echo time of the NMR tool. Since no magnetic field gradient is enforced in the simulations, the signal generated by fluid protons is simply proportional to the population of magnetized protons sampled with period TE . The First-Passage-Time method is particularly suited for the simulation of proton displacements in large pore spaces as it allows the simulation of large displacements in a few steps. However, close to surfaces of material discontinuity, the First-Passage-Time strategy does not converge and instead a conventional random walk of fixed step ϵ is necessary.

If contact is made with a surface of material discontinuity, then the proton magnetization decays with a probability equal to

$$p = \frac{\rho\epsilon}{D_o}, \quad (2)$$

where ρ is the surface relaxivity of the interface (Bergman et al., 1995). If no magnetization decay occurs, then the proton rebounds randomly at the surface of the interface.

Once a large-enough number of proton trajectories are simulated with the Monte Carlo algorithm, convergence to the average time solution is insured and the total magnetization signal can be inverted into a T_2 distribution (generally a few hundreds to a thousand proton trajectories are needed for statistical convergence, depending on the modeled pore-size distribution).

The total relaxation of the pore fluid is generally considered equal to

$$T_2 = (1/T_{2S} + 1/T_{2B})^{-1} = (\rho S/V + 1/T_{2B})^{-1}, \quad (3)$$

where T_{2S} is the surface relaxation, T_{2B} is the bulk relaxation,

ρ is the pore surface relaxivity, and S/V is the pore surface-to-volume ratio. Considering equation (3), we remark that the dual random-walk algorithm introduced by Ramakrishnan et al. (1999) only models the effect of T_{2S} . Because T_{2B} is solely a function of fluid properties, we propose to take into account bulk relaxation effects by multiplying the simulated magnetization decay by the TE -sampled temporal decay $\exp(-t/T_{2B})$ before performing the T_2 inversion. An in-depth description of this algorithm including benchmark examples and extensions to consider the effect of a constant external magnetic field gradient can be found in Toumelin (2002), and Toumelin et al. (2002).

ADAPTATION OF THE SIMULATION MODEL TO REPLICATE THE NMR RESPONSE OF FLUIDS IN ROCK SAMPLES

The purpose of the simulation work is to ascertain the influence of pore coupling on the NMR response of the available core samples. Once the proportion of actively coupled pores has been quantified for each sample, the main task is to determine the bimodal pore model that honors the NMR measurements.

On the hydraulic isolation of vuggy porosity

For every sample, the irreducible water saturations S_{wir} measured by NMR is larger than the fractional micro-

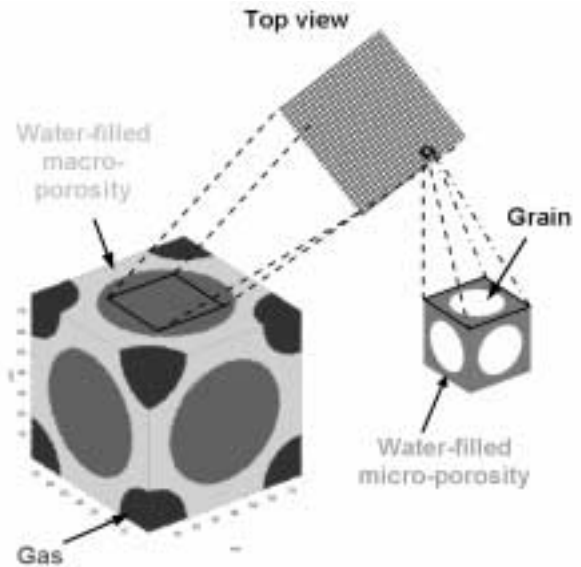


FIG. 9 Three-dimensional representation of the distribution of fluids and rock matrix at the spatial resolution of both macro- and micro-cells. Gas blobs are centered on the intergranular macro-pores. Compaction is simulated by including sphere diameters larger than the concentric cube sizes.

porosity ϕ_{micro}/ϕ_T . Therefore, we can assume that the entire water-wet micro-pore region is filled with connate water, and that the complementary amount of irreducible water ($S_{wir}\phi_T - \phi_{micro}$) resides in other porosity regions. However, the pore analysis defines the vuggy pores (pore mode 2) as isolated and sealed by cementation. In other words, under this assumption, no fluid can leave the vuggy macro-pores unless the rock is fractured.

Analysis of the NMR experimental results in Figure 8 shows that, for each sample, the long- T_2 peak, corresponding to the water-filled vugs at $S_w = 1$, disappears at S_{wir} . This implies that the water-filled vugs were effectively drained by centrifugation. Such an observation, in turn, contradicts the initial assumption that the long- T_2 peak is associated with hydraulically isolated vugs. Thus, NMR measurements on the three available cores strongly suggest that vugs observed at SEM resolution may not be totally isolated hydraulically from the rest of the porous network.

Determination of the model parameters

By describing “vugs” as part of a coupled pore system, their NMR response can be explained by the superposition of coupled modes. We assume that the total NMR response of the porous medium is dictated by the collective response of porosity modes that are, from a diffusive viewpoint, coupled by pairs of two modes. Such an assumption is of course amenable to our numerical simulation algorithm. For instance, the macro-porosity regions (modes 1 and 2) are

expected to couple with the pores of mode 3 (peripheral porosity located between the cement crystals) more than with those of mode 4 (intrinsic micro-porosity). By contrast, the two macro-porosity modes are expected to exhibit no mutual coupling.

In order to be consistent with experimental results, we choose the average radii and porosities of the main pore modes as input parameters. The pore information for modes 1 through 3 is adapted from the pore-size distribution analysis. However, the average radius of mode 4 micro-pores has to be determined for each sample so that it honors the spatial range observed on the corresponding SEM images, and at the same time remains consistent with the NMR measurement. Furthermore, as shown by Ramakrishnan et al. (1999), the influence of the rock surface relaxivity ρ (defined as the inverse of the product of T_{2S} and the surface-to-volume ratio S/V of the pore) is crucial to the NMR response of pores exhibiting diffusion coupling. In sandstones, an estimate for ρ can be obtained from the quasi-linear relationship between T_{2S} and S/V . By contrast, the presence of diffusion coupling in carbonates prevents a simple determination of ρ . The choice of NMR parameters in our simulation model therefore represents an iterative process with two degrees of freedom, namely, the average micro-porosity radius r_4 , and the surface relaxivity ρ . A practical way to solve for the required parameters is to utilize the NMR responses of the desaturated samples.

Sample A

The NMR measurements performed on Sample A yielded a high irreducible water saturation of 52.4%. This value is larger than the fractional micro-porosity $\phi_4/\phi_T = 42.4\%$, thereby implying that, at S_{wir} , the detected NMR signal is produced by water within both the micro-porosity (mode 4) and the next bigger pores of mode 3. Therefore, the selection of the equivalent model consisted of finding a satisfactory combination of (r_4, ρ) couplet, such that the bimodal porosity simulation constructed with the remaining parameters ($\phi_4 = 9.8\%$, $\phi_3 = 3.8\%$, $r_3 = 6 \mu\text{m}$) matched the NMR measurements shown in Figure 8 at S_{wir} . Simulation models were tested for $r_4 = 0.2, 0.4$ and $0.5 \mu\text{m}$, and for $\rho = 1, 2, 3$, and $5 \mu\text{m/s}$, corresponding to usual values for carbonate rocks. The irreducible water saturation was matched by defining a gas blob radius within the intergranular porosity region of the model representing pore mode 3, where the surface relaxivity at the gas/water interface was taken equal to zero. Given the low gas hydrogen index, it was assumed that the pore volume associated with gas created no magnetization signal. A best fit was obtained for $r_4 = 0.5 \mu\text{m}$ and $\rho = 2 \mu\text{m/s}$, and by assuming a gas blob of radius equal to $6 \mu\text{m}$.

The model was then tested for the remaining porosity

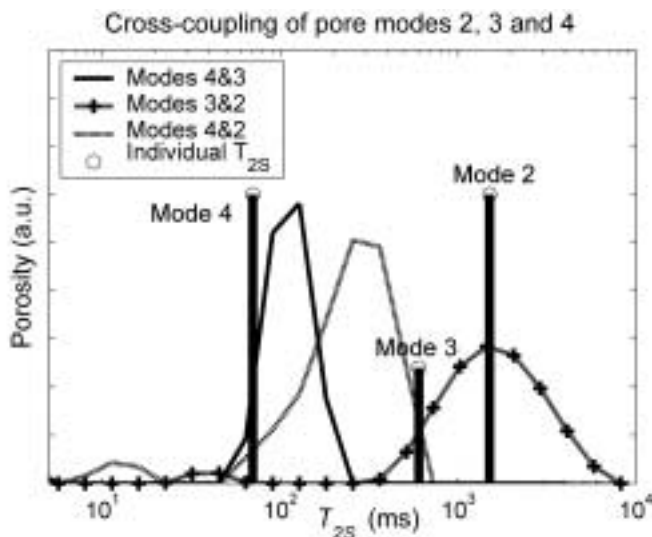


Fig. 10 Cross-coupled NMR responses of the main pore modes present in sample A, and comparison with the uncoupled modes. Stems represent the individual T_{2S} response of each mode in the absence of coupling, that is, the ‘original’ location of the T_{2S} peaks before diffusive pore coupling.

modes. Figure 10 shows the cross-coupled NMR responses corresponding to modes 2, 3 and 4, where each coupled mode pair is weighted by its total porosity. If the pore system were completely uncoupled, its NMR response would be obtained from the superposition of the T_{2S} values of its main pore modes. In Figure 10, the individual T_{2S} response of each mode is described in a way that allows qualitative assessment of the coupling effect between each mode pair. It can be seen that mode 3 only slightly influences the remaining pore modes by causing no appreciable T_2 distribution shift. Consequently, the response of the whole pore system can be explained as controlled mainly by the coupling between the intra-granular micro-porosity (mode 4) and the vuggy porosity (mode 2). A reasonable approximation of the sample NMR response can then be obtained by considering the coupled response of modes 2 and 4 at $S_w = 1$, weighted by the total porosity of the sample. The T_2 distribution of the corresponding simulation model compares extremely well with the measurements (see Figure 11). Locations for the peaks on the T_2 spectra match quantitatively. We remark that the width of the micro-porosity peak is narrower in the numerical simulation than in the real rock because the simulation includes a single micro-pore size whereas the real rock includes a distribution of sizes. This exercise validates the S_{wir} -based parameters and the assumption of full diffusion coupling between existing pores.

Sample B

A similar approach was used to construct a model that could replicate the NMR response of the apparently partially coupled core sample B. However, the coupling process in this sample is markedly more complex than in the case of sample A. An iterative process is needed to accurately model the corresponding NMR response. Sample B exhibits an irreducible water saturation, $S_{wir} = 27.7\%$, which falls remarkably close to its fractional micro-porosity, $\phi_4/\phi_T = 26.3\%$. Consequently, it was assumed that the irreducible water saturation was located within the micro-porous region only, and that the corresponding NMR signal could be modeled with a unimodal pore system. The micro-pore size r_4 of the model was calibrated to $0.45 \mu\text{m}$ so that the individual response of mode 4 matched the NMR measurement performed at S_{wir} assuming a surface relaxation of $2 \mu\text{m/s}$. In this sample, however, three additional coupled pore modes contribute to the NMR response at higher water saturations, so that the pore coupling process requires some simplifications.

The first stage of the iterative simulation procedure assumed that diffusion was controlled by direct diffusive coupling between all pore modes except modes 3 and 4.

Figure 12 shows the simulation results obtained with these cross-coupled modes. The simulations were performed by taking into account the porosities associated with each pair of pore modes, along with their individual T_{2S} response when regarded as uncoupled. As can be seen in this figure, the overall magnetization associated with the micro-porosity (mode 4) consistently remains close to that obtained in the absence of diffusive coupling. However, the magnetizations borne by the macro-porosities (modes 1 and 2) shift to lower relaxation times, spread over the whole T_{2S} range of the macro-porosities, and slightly fill the gap with mode 4. The coupling process occurring over the entire pore system of this sample is expected to enhance the two T_2 peaks centered at 70 and 2000 ms, before accounting for bulk relaxivity, with a valley of T_2 relaxations between the two peaks. As an illustration, Figure 13 provides a comparison of the experimental NMR T_2 distribution with the T_2 distribution inverted from the sum of the coupled simulation results used to construct Figure 12 (obtained by assuming a brine bulk relaxation of 2300 ms). Figure 13 shows clearly that the superposition of the coupled NMR responses is a good approximation to the NMR measurements.

Further successive simulation steps would be required to bridge the gap between the two measured T_2 peaks and to accurately reproduce the NMR measurements. These steps

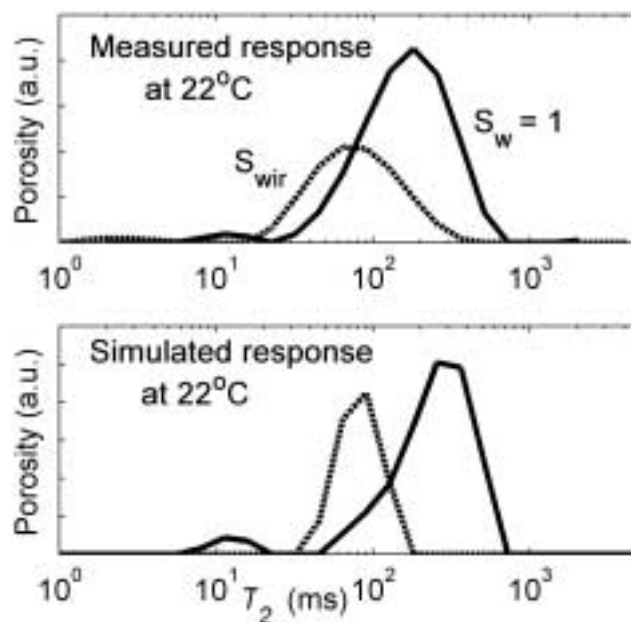


FIG. 11 Comparison of simulations and measurements of sample A at room temperature. Solid curves: $S_w = 1$. Dashed curve: $S_w = S_{wir}$. Although sharper than the experimental peak at irreducible water saturation, the simulation result honors both the T_2 peak value and the porosity.

would need to consider equivalent bimodal models based on the T_2 distribution yielded by the previous simulation step. For example, because it originates from the coupling between both Modes 2 and 3 (Figure 12a) and Modes 4 and 2 (Figure 12b), a strong T_2 decay mode appears after the first iteration around 1000 ms that does not correspond to the initial pore-size distribution. The next step of the process would include the simulation of the coupling relationship between this 1000-ms T_2 mode and the one at 50 ms that results from the coupling of Mode 4 to other modes in the first iteration. This simulation would create a strong T_2

mode at approximately 300 ms, similar to that observed after coupling between Modes 3 and 4. When applied to all the decay rates obtained from the previous simulation step, this process would yield the T_2 values required to bridge the T_2 gap between the two peaks exhibited by the measurements. Such an exercise, however, is beyond the scope of this paper.

Sample C

The third sample studied in this section is the one exhibiting the most macro-porosity and peripheral cementation, and no apparent sign of diffusive coupling. We used this example of an uncoupled sample to contrast the simulation results with those of the coupled samples, A and B, and to determine the behaviors which more specifically characterize coupled systems.

In summary, the simulation models helped us to determine coupled pore geometry for both samples A and B. These models validated the pore-size distributions determined by core image analyses. By keeping the same pore-size distributions and by preventing the diffusion coupling between the pore modes, equivalent uncoupled models were constructed for samples A and B. Simulation through these uncoupled models yielded equivalent uncoupled responses that reproduced what the NMR response of sam-

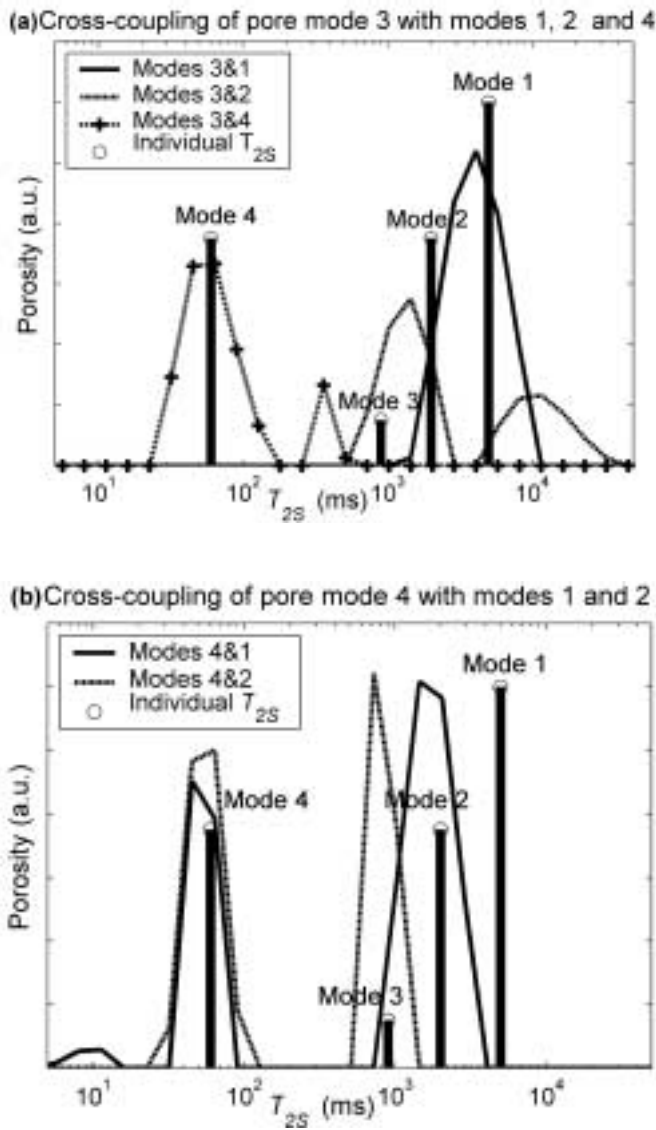


FIG. 12 Cross-coupled NMR responses of the main modes present in sample B and comparison with the uncoupled modes. Stems represent the individual T_{2S} response of each mode in the absence of diffusive coupling.

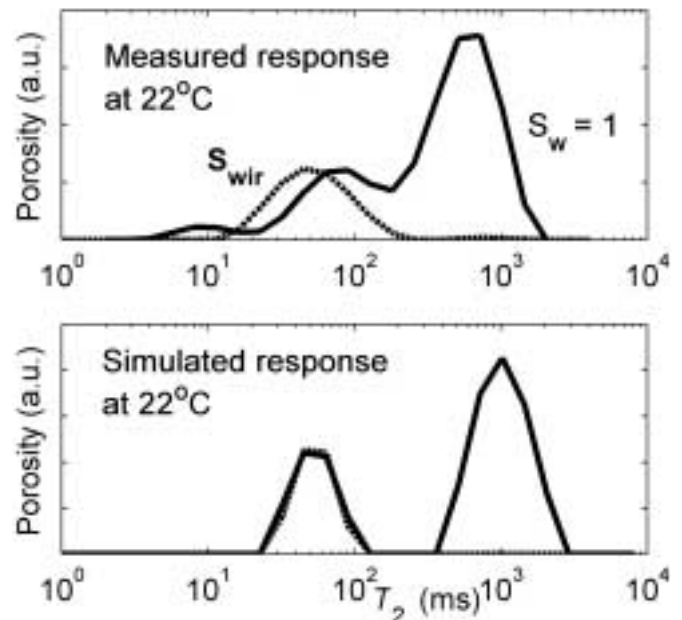


FIG. 13 Comparison of simulations and measurements of sample B at room temperature. The closest representation of this sample's structure after the first iteration of the numerical model exhibits negligible diffusive coupling.

ples A and B *would have been* like in the absence of diffusion coupling. These uncoupled responses are subsequently used to assess the impact of diffusion coupling on the estimation of BVI.

ANALYSIS OF SENSITIVITY OF NMR MEASUREMENTS TO TEMPERATURE

Equation (3) assumes that the behavior of the total transverse relaxation with respect to temperature can be attributed to the following factors:

- a) The bulk relaxation T_{2B} , roughly proportional to temperature and inversely proportional to fluid viscosity.
- b) The surface relaxivity ρ , whose dependence on temperature is governed by the magnetic content of the rock's mineralogy and fluid types (Godefroy et al., 2001).
- c) The effective surface-to-volume ratio S/V surrounding the protons of the fluid.

Without alternative means to study the effect of temperature on surface relaxivity, we discuss the relative importance of the above factors (a) and (c), based on NMR measurements performed on eight carbonate samples gathered within the same well, and on numerical simulations.

Role of T_{2B}

Three of the eight samples are Samples A, B, and C described in the previous sections, along with five other samples that were selected at a later stage of the study, henceforth referred to as additional samples. As previously described, measurements on samples A, B and C were performed at the temperatures of 4–10°C, 22°C, 45°C, and 60–65°C. Measurements on the additional samples were also performed at 1°C, 22°C, and 60°C.

Figure 14 shows the T_2 distributions of samples A, B and C at the minimum and maximum measured temperatures. We remark that the degree of temperature dependence varies from sample to sample despite the fact that the saturation fluid is the same (brine) for all the samples. Similar observations were made on the additional samples, but no universal temperature dependency was found. However, for the samples exhibiting temperature dependence, relaxation times T_2 consistently increased with temperature.

At each temperature T , and for each sample, the geometric mean of the experimental T_2 distribution was computed as the measured T_2 value. Then, in order to assess the influence of the aforementioned factors (b) and (c) (i.e., surface relaxivity and effective surface-to-volume ratio), we subtracted the effect of bulk relaxation T_{2B} from the measured T_2 value to obtain an equivalent surface relaxation, i.e.,

$$T_{2S}(T) = (1/T_2(T) - 1/T_{2B}(T))^{-1} \quad (4)$$

For all the samples of this study, the values of T_{2S} and T_2 are plotted with respect to temperature in Figure 15. We observe that the role played by T_{2B} is rather significant for the samples that exhibit moderate temperature sensitivity (namely, samples B and C). However, for the samples that exhibit the largest temperature dependence (such as the additional samples), the role of T_{2B} is negligible and does not explain the systematic increase of T_2 with T . In the current absence of more detailed information on the structure of the additional samples, no systematic conclusion can be drawn to assess the relationship between coupling and dispersion of T_2 with temperature.

Role of effective S/V

Next, we address the issue of the sensitivity of the effective surface-to-volume ratio to temperature changes. In an isolated pore model, the S/V of an individual pore does not

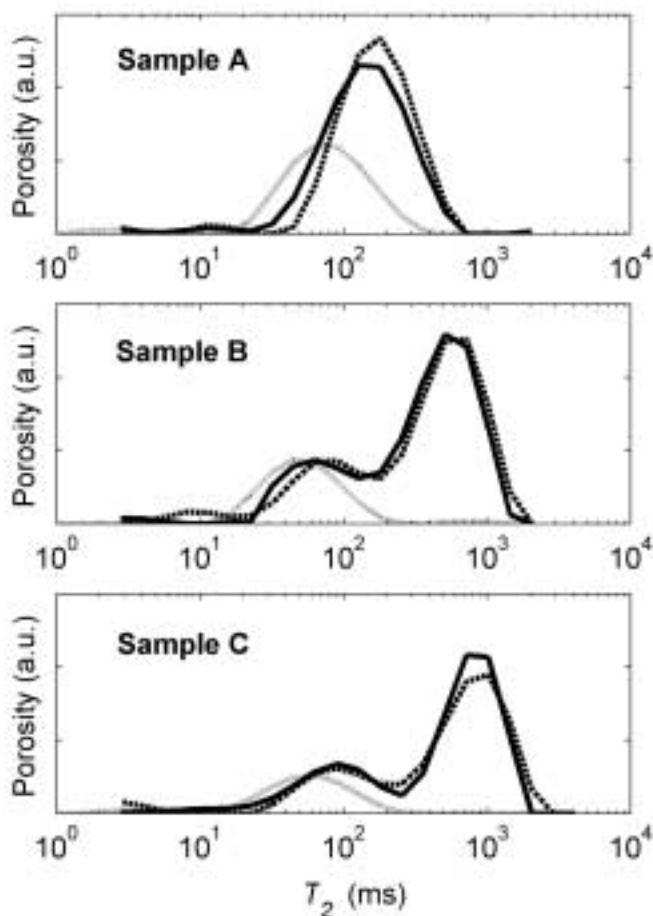


FIG. 14 Examples of T_2 distributions measured at 4 and 65°C for samples A, B and C. Solid curves: NMR response at $S_w = 1$ and 4–10°C; dashed curves: $S_w = 1$ and 60–65°C; dotted curves: $S_w = S_{wir}$ and 22°C.

change with temperature. In a coupled pore model, however, the S/V of an individual pore is no longer independent of other pores. Therefore, an effective S/V concept is necessary to take into account the coupling effect. Ramakrishnan et al. (1999) showed how the presence of diffusive coupling could modify the effective S/V for given diffusion lengths of the medium. We recognize that temperature can also modify this effective S/V when diffusive coupling is present. Indeed, when temperature, and hence bulk diffusivity, increases, the probability of proton exchange between the different pore modes increases as well. In turn, the effective surface-to-volume ratio of the pore volume departs from its geometrical value. For instance, protons within the micro-porous regions are prone to diffuse further within the macro-pore region when temperature increases, and therefore the effective S/V “seen” by these protons decreases. Similarly, when temperature increases, the protons within the macro-pore regions are more likely to reach the micro-porous regions and therefore their effective S/V increases. However, both phenomena do not necessarily cancel each

other, since quantitatively the S/V decrease in larger pores cannot compensate the S/V increase in smaller pores. Consequently, the effective S/V behavior of such coupled systems will be dominated by proton behavior within the micro-porous regions.

We support this statement with simulations made with the three cross-coupled pore models of sample A, for temperatures of 4 and 65°C, and a constant surface relaxivity $\rho = 2 \mu\text{m/s}$ estimated during the calibration process of the simulation model with the core data. The simulated T_{2S} results, independent of bulk effects, are plotted in Figure 16 and are compared to the ones previously obtained at room temperature (Figure 10). In Figure 16, we observe that temperature does affect the coupled responses between the respective pores modes: T_{2S} decreases slightly with temperature.

Unresolved technical issues

This coupling influence, however, cannot explain the temperature behavior observed in Figure 15. Indeed, this

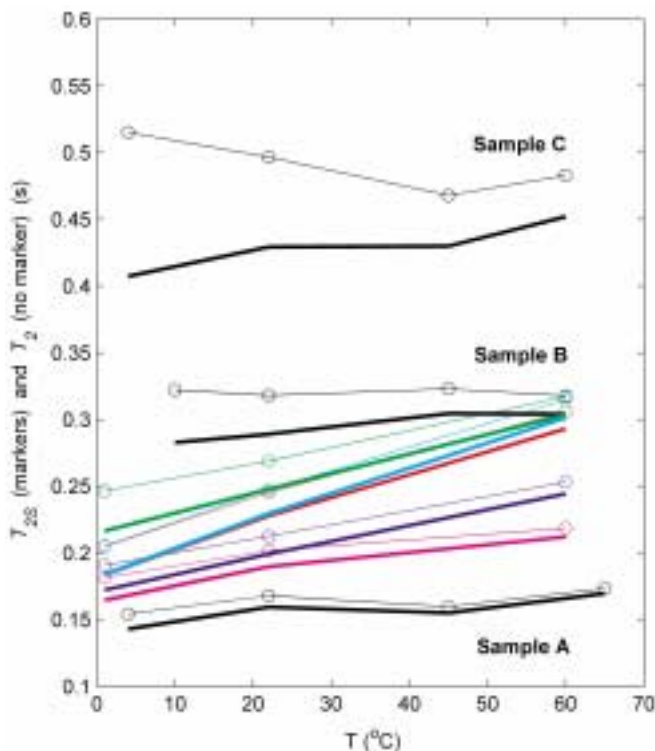


FIG. 15 Diagram showing the experimental influence of temperature on the NMR response in carbonate samples gathered from the same well. Black lines: measurements of samples A, B and C; colored lines: measurements of the five additional samples from the same well. Lines without markers represent the total measured response, whereas those with circles correspond to equivalent surface relaxation.

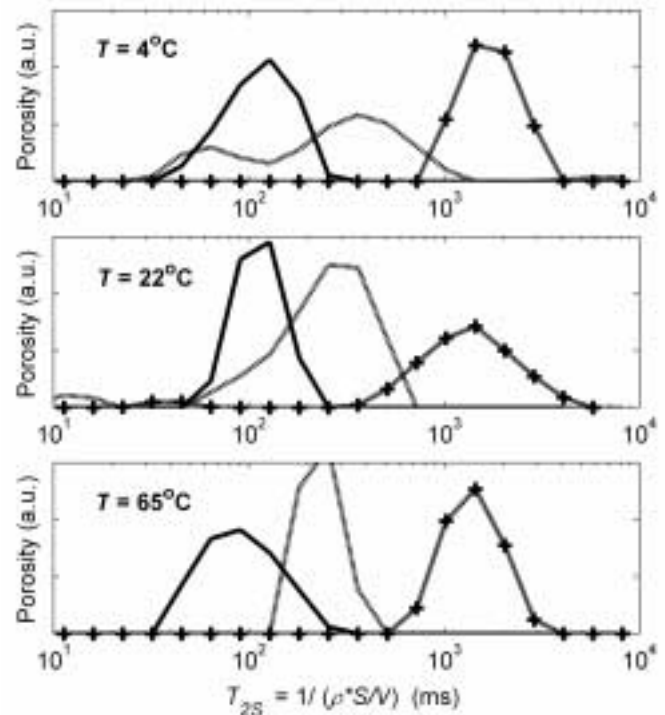


FIG. 16 Numerical evidence for the influence of temperature on the effective surface-to-volume ratio of diffusively coupled pore systems. These results of simulating bimodal models of sample A assume a constant, uniform surface relaxivity $\rho = 2 \mu\text{m/s}$, at temperatures of 4, 22, and 65°C. (Refer to Figure 10.) In all the cases, the surface relaxation times T_{2S} slightly decrease with temperature.

TABLE 1 $BVI (= \phi S_{wir})$ errors due to diffusion coupling applying a conventional 90-ms $T_{2cutoff}$ at ambient temperature.

Parameter	Sample A	Sample B	Sample C
Correct S_{wir}	52%	28%	24%
S_{wir} determined from measurements	27%	22%	18%
<i>Percent error in S_{wir}</i>	48%	21%	24%
S_{wir} determined from decoupled simulations	52%	29%	–
<i>Percent error in S_{wir}</i>	0%	3%	–

phenomenon should justify the observation that, when T decreases, T_{2S} increases more conspicuously when coupling is present than when it is absent. Yet, we observe the opposite trend in Figure 15. This implies that the effect of coupling on the effective S/V is of secondary order, and that an adverse phenomenon not accounted for takes place here. If we rely on the assumptions made by equation (3), then such a temperature dependence is likely to be dominated by the behavior of ρ with temperature when surface relaxivity is heterogeneous within the formation. We realize that this proposition needs further experimental verification. However, the experimental means necessary to undertake such a study are at this moment unavailable in our laboratory.

INFLUENCE OF TEMPERATURE AND DIFFUSIVE COUPLING ON BOTH T_2 -CUTOFF, BVI, AND PERMEABILITY

This section presents results based (a) on the comparison between measurements performed at different temperatures to quantify the impact of temperature, and (b) on the comparison between measurements and simulations at ambient temperature to quantify the impact of coupling. In Figure 17, we plot the cumulative porosity distributions for samples A, B and C at 100% water saturation at room temperature and the two extreme temperatures that were measured, as well as at S_{wir} measured at room temperature. The current practice of core-NMR based $T_{2cutoff}$ employs measurements performed at ambient conditions. Neglecting the temperature dependence of the T_2 distribution could introduce substantial errors. In what follows, we provide a series of comparisons aimed at illustrating possible biases on BVI and permeability estimates associated with high and low temperature data when assuming parameters derived from

ambient conditions. Figure 17 also shows the response simulated at ambient temperature for equivalent uncoupled models of Samples A and B, determined from the rock structures inferred in the first parts of this paper.

Tables 1 to 4 interpret the curves in Figure 17 to quantify the effect of temperature and diffusive coupling on BVI (or S_{wir}) and permeability, by comparing the Timur-Coates and the $T_{2logmean}$ permeability models associated with the three samples. (See Kenyon, 1997, for a discussion of these models.) In each table, the percentages shown in *italic* represent the relative errors of the estimated properties.

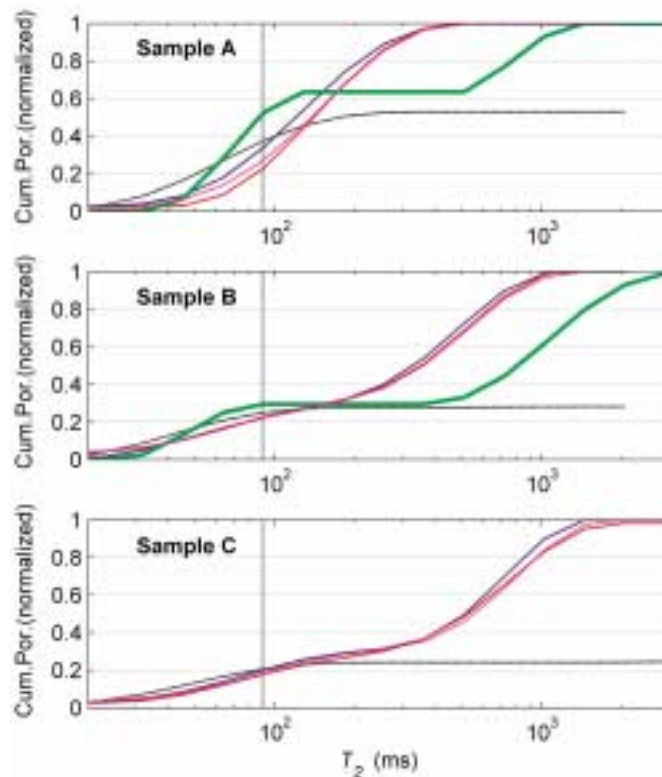


FIG. 17 Cumulative porosity plots of the T_2 distributions of samples A, B and C at different temperatures. Blue curves: cumulative porosity curves obtained from the NMR response at $S_w = 100\%$ and 4°C; dashed magenta curves: at $S_w = 100\%$ and 22°C; red curves: at $S_w = 100\%$ and 65°C; black dotted curves: at $S_w = S_{wir}$ and 22°C; green curves: simulated responses of the corresponding diffusively uncoupled models (samples A and B only) at $S_w = 100\%$ and 22°C. Vertical lines at 90 ms represent the BVI- $T_{2cutoff}$ conventionally used for carbonate rocks.

TABLE 2 Correct $T_{2cutoff}$ for BVI and Timur-Coates permeability model.

Parameter	Sample A	Sample B	Sample C
Coupling effect (at ambient temperature):			
Correct $T_{2cutoff}$ (ms) from measurements (allowing coupling)	143	139	–
Correct $T_{2cutoff}$ (ms) from decoupled simulations	92	83	–
Temperature effect (from measurements):			
Correct $T_{2cutoff}$ (ms) at low temperature (4–10°C)	126	138	120
Correct $T_{2cutoff}$ (ms) at high temperature (60–65°C)	145	129	151

BVI errors

The actual value of S_{wir} (or BVI percentile, since $BVI = \phi S_{wir}$) of each sample is defined by the maximum normalized cumulative porosity read from measurements made on the centrifuged core sample,

$$S_{wir} = \frac{\int_{T_{2min}}^{T_{2max}} P'(T_2) dT_2}{\phi}, \quad (6)$$

where P' is the T_2 distribution of the centrifuged core sample.

For each sample and each experiment made at 100% water saturation, the value of S_{wir} can also be determined by

$$S_{wir} = \frac{\int_{T_{2min}}^{T_{2cutoff}} P(T_2) dT_2}{\int_{T_{2min}}^{T_{2max}} P(T_2) dT_2}, \quad (5)$$

where P is the T_2 distribution of the fully saturated sample, and the denominator represents the porosity of the sample. Alternatively, by taking the value of S_{wir} found on the centrifuged samples, we can calculate the correct $T_{2cutoff}$ to be used for each sample at ambient temperature.

Table 1 quantifies the error due to diffusion coupling when the nominal 90-ms cutoff expected for carbonate rocks is used to interpret the NMR data. We can observe a substantial 48% BVI error associated with such a generic

TABLE 3 BVI and permeability errors due to temperature, associated with Timur-Coates permeability model.
$$k_{Coates} = C_c \phi^4 (BVM / BVI)^2 = C_c \phi^4 ([1 - S_{wir}] / S_{wir})^2$$

Parameter	Sample A	Sample B	Sample C
Correct S_{wir}	52%	28%	25%
Correct AT $T_{2cutoff}$ (ms) (ambient temp.)	143	139	137
LT S_{wir} (low temperature)	60%	27.5%	26.5%
HT S_{wir} (high temperature)	51%	28.5%	23.5%
S_{wir} relative error due to temperature	15%	2%	6%
ϕ	23.6%	19%	21.2%
C_c (D)	1.51	8.12	53.91
Correct k (mD)	4	70	980
LT k_{Coates} (mD) (low temperature)	2	74	838
HT k_{Coates} (mD) (high temperature)	4.3	67	1154
k_{Coates} relative error due to temperature	50%	5%	18%

cutoff for Sample A, and relatively high errors (larger than 20%) for Samples B and C. However, if we assess the irreducible water saturation using the same cutoff for the uncoupled models of Samples A and B, then we obtain values that are remarkably close to the actual irreducible saturations. This observation validates for these two samples the usage of the standard 90 ms cutoff in the absence of diffusion coupling. It also corroborates the pore-size models when the latter are uncoupled. The large errors calculated from the measurements on the real rocks (allowing diffusion coupling) clearly suggest the need to account for diffusive coupling in the interpretation of NMR data. Introducing the notion of coupling/decoupling here dramatically reduced the discrepancies of BVI estimates for Samples A and B.

Similar results are shown in Table 2, where we assessed how large a variation of $T_{2cutoff}$ was required to obtain correct values of BVI (as well as permeability using the Timur-Coates model). This exercise focused on both the temperature differences of the measurement, and the decou-

pling allowed by the simulations. In Table 2, the correct cutoff values in case of decoupled pores in samples A and B (i.e., if no diffusion coupling was present) are very close to the 90-ms cutoff previously mentioned. However, the proximity of the correct cutoff values for samples A and C suggests that $T_{2cutoff}$ does not necessarily depend on the degree of diffusion coupling exhibited by the pore structure of the samples.

Similarly, Table 2 shows that temperature causes a remarkable shift of the correct $T_{2cutoff}$ by 10 to 30 ms. Table 3 provides estimations of errors when the cutoff is individually determined from the measurement of each sample A, B, and C, at ambient temperature (AT: 22°C), and when these cutoffs are applied to the measurements performed at low temperature (LT: 4 to 10°C, depending on the sample A, B, or C) and high temperature (HT: 60 to 65°C). One could expect such cutoff values to yield accurate estimates of BVI and BVI-based permeabilities. However, a maximal BVI relative error of 15%, accounting for as high as 8% of the pore volume, was obtained on the temperature range used in the measurements of sample A. Discrepancies even larger than the above could be expected for larger temperature intervals. This analysis proves the rather high inaccuracy of cutoffs derived at ambient-temperature.

Permeability errors

The Timur-Coates permeability model was first used to assess permeability from BVI estimates at the extreme measured temperatures. Results are shown in Table 3, along with those of BVI described in the previous section. Because all three samples A, B and C exhibit different pore structures, we allowed the constant C_C in the Timur-Coates permeability model to vary from sample to sample. For each sample, C_C was calculated from the measured values of permeability (k) and porosity (ϕ), and from the values of S_{wir} just estimated from ambient-temperature (AT: 22°C) $T_{2cutoff}$ s. Then, using these irreducible saturations and the true values of ϕ , Table 3 shows the resulting values of k for low and high temperatures. The maximal error percentage caused by the use of room-temperature parameters reached 50% for Sample A and 18% for Sample C. We observe that the high relative error obtained for sample A actually corresponds to a low absolute error of 2 mD.

Table 4 shows the results obtained with the $T_{2logmean}$ permeability model. As in the case of Table 3, the permeability values described in Table 4 were calculated for the constant C_S at ambient temperature, based on the measured logarithmic means of the T_2 distributions. All the samples exhibit relative errors in permeability close to 15%. Therefore, this permeability model shows slightly less stability with temperature than the Timur-Coates model. Such behavior is

TABLE 4 $T_{2logmean}$ and permeability errors using $T_{2logmean}$ model $k_{T_{2logmean}} = C_S \phi^4 (T_{2logmean})^2$.

Parameter	Sample A	Sample B	Sample C
ϕ	23.6%	19%	21.2%
C_S (D/s ²)	67.71	414.46	1530.61
Measured			
AT $T_{2logmean}$ (ms) (ambient temp.) (allowing coupling)	138	360	563
Simulated			
AT $T_{2logmean}$ (ms) (ambient temp.) (preventing coupling)	88	821	–
Measured			
LT $T_{2logmean}$ (ms) (low temperature)	127	332	517
Measured			
HT $T_{2logmean}$ (ms) (high temperature)	142	353	531
Correct k (mD)	4	70	980
LT $k_{T_{2logmean}}$ (mD) (low temperature)	3.4	60	826
HT $k_{T_{2logmean}}$ (mD) (high temperature)	4.2	67	872
$k_{T_{2logmean}}$ relative error due to temperature	15%	14%	16%

consistent with the remark just made concerning Sample A. It is noticeable that most hydrocarbon reservoirs exhibit higher temperatures than those reported in this study, in which case permeability errors will be larger than those shown in Table 3 and 4.

A substantial difference of $T_{2logmean}$ between measurements and decoupled simulations is also noted in Table 4. It is remarkable that Sample A was the sample that exhibited the largest BVI error due to coupling (see Table 1), hence the largest discrepancy with a BVI-based permeability model, whereas it is Sample B that exhibits the largest $T_{2logmean}$ error, hence the largest discrepancy with a $T_{2logmean}$ -based permeability model. However, because in practice different constants would be required for each sample, we choose not to show calculations of such coupling-induced permeability errors in this paper.

SUMMARY AND CONCLUSIONS

A study has been presented of experimental NMR measurements based on three carbonate samples and complemented by numerical time-domain simulations. The study made use of SEM images to provide a priori models of pore structures for the simulations. Our simulation model incorporates diffusion coupling between pores with different length scales. NMR core measurements were conducted on the same samples to validate the simulation models and to assess the diffusion processes taking place within the pore structure. The simulations were then used to predict the NMR response of the samples in the absence of diffusive coupling. These decoupled simulations provided a basis for comparison with the measurements, which naturally include coupling. It has been shown that the inclusion of diffusion coupling could improve (a) the interpretation of the carbonate pore structure, (b) the estimation of pore size and T_2 distribution, and (c) the understanding of discrepancies in $T_{2\text{cutoff}}$ and BVI estimates.

Analysis of measurements performed at temperatures from 4 to 65°C showed that the generally unaccounted temperature effects on bulk relaxation T_{2B} could be a primary cause for NMR temperature dependence when diffusion coupling is weak. We also remarked that the strength of diffusion coupling is influenced by temperature. However, both bulk and diffusive coupling could not completely explain the temperature dependence of the NMR responses that was measured in the samples.

Finally, a quantitative estimate has been made of the errors associated with the estimations of BVI and permeability when both diffusion coupling and temperature variations are neglected. We showed that the 90-ms cutoff conventionally used for carbonate rocks remained accurate for the three samples, under the condition that no diffusive coupling was present. Hence, coupling effects must be included in an accurate interpretation of NMR measurements. It was also found that calibrating the permeability models with measurements performed at ambient temperature could lead to relative errors of at least 15% for the temperature interval considered in this study.

NOMENCLATURE

AT	ambient temperature (22°C)
BVI	immovable fluid volume in place ('bound volume irreducible')
C_C	constant for the Timur-Coates permeability model (D), $1D = 0.987 \cdot 10^{-12} \text{ m}^2$
C_S	constant for the $T_{2\text{logmean}}$ permeability model (D/s^2)
D_o	bulk diffusivity ($\mu\text{m}^2/\text{ms}$)

HT	high temperature of the measurements (60 to 65°C)
k	permeability (mD), $1\text{mD} = 0.987 \cdot 10^{-15} \text{ m}^2$
LT	low temperature of the measurements on samples A, B and C (4 to 10°C)
p	probability of proton demagnetization at a fluid interface
P, P'	T_2 distributions corresponding to fully saturated and irreducible saturation states, respectively
R	macroscopic displacement of a step of First-Passage-Time technique (nm)
S/V	surface-to-volume ratio of pore ($1/\mu\text{m}$)
S_w	water saturation in a core sample
S_{wir}	irreducible water saturation
T	temperature (°C)
t	time (ms)
T_2	total NMR transversal relaxation time (ms)
T_{2B}	bulk NMR transversal relaxation time (ms)
$T_{2\text{cutoff}}$	relaxation value at which the cumulative NMR porosity equals BVI (ms)
$T_{2\text{logmean}}$	logarithmic mean of the T_2 distribution (ms)
T_{2S}	surface NMR transversal relaxation time (ms)
TE	echo time of the NMR tool (ms)
Δt	time duration associated with a First-Passage-Time technique step (ms)
ε	unitary displacement of a step of conventional random-walk technique applied near the pore wall (nm)
ρ	surface relaxivity ($\mu\text{m/s}$)
ϕ	porosity

ACKNOWLEDGMENTS

We express our gratitude to Baker Atlas for permission to publish these results, and for partial funding through summer internship positions offered to ET and DMF in 2001. A note of gratitude goes to Drs. Gigi Zhang and Carl Edwards for useful technical discussions. The help of Julian Singer and the anonymous reviewers of *Petrophysics* was also greatly appreciated to finalize this paper. We acknowledge partial support from the Center of Excellence in Formation Evaluation of The University of Texas at Austin, and from the American Chemical Society under grant ACS PRF#37519-AC9. The Center of Excellence in Formation Evaluation is an industry research consortium jointly sponsored by Baker Atlas, Halliburton, Schlumberger, and Anadarko Petroleum Corporation.

REFERENCES

- Allen, D. F., Boyd, A., Massey, J., Fordham, E. J., Amabeoku, M. O., Kenyon, and W. E., Ward, W. B., 2001, The practical appli-

- cation of NMR logging in carbonates: 3 case studies, paper K, in 42nd Annual Logging Symposium Transactions: Society of Professional Well-Log Analysts.
- Anselmetti, F. S., Luthi, S., and Eberli, G. P., 1998, Quantitative characterization of carbonate pore systems by digital image analysis: AAPG Bulletin, vol. 82, no. 10, p. 1815–1836.
- Bergman, D. J., Dunn, K.-J., Schwartz, L. M., and Mitra, P. P., 1995, Self-diffusion in a periodic porous medium: a comparison of different approaches: *Physical Review E*, vol. 51, no. 4, p. 3393–3400.
- Chen, S., Fang, S., Georgi, D., Salyer, J., and Shorey, D., 1999, Optimization of NMR logging acquisition and processing, SPE-56766, in SPE Annual Technical Conference and Exhibition Proceedings: Society of Petroleum Engineers.
- Godefroy, S., Fleury, M., Deflandre, F., and Korb, J.-P., 2001, Temperature effect on NMR surface relaxation, SPE-71700, in Annual Technical Conference and Exhibition Proceedings: Society of Petroleum Engineers.
- Kenyon, W. E., 1997, Petrophysical principles and applications of NMR logging: *The Log Analyst*, vol. 38, no. 2, p. 21–43.
- Prior, D. J., Boyle, A. P., Brenker, F., Cheadle, M. C., Day, A., Lopez, G., Peruzzo, L., Potts, G. J., Reddy, S., Spiess, R., Timms, N. E., Trimby, P., Wheeler, J., and Zetterström, L., 1999, The application of electron backscatter diffraction and orientation contrast imaging in the SEM to textural problems in rocks: *American Mineralogist*, vol. 84, p. 1741–1759.
- Quintero, L., Boyd, A., Gyllensten, A., and El Wazeer, F., 1999, Comparison of permeability from NMR and production analysis in carbonate reservoirs, SPE-56798, in Annual Technical Conference and Exhibition Proceedings: Society of Petroleum Engineers.
- Ramakrisnan, T. S., Schwartz, L. M., Fordham, E. J., Kenyon, W. E., and Wilkinson, D. J., 1999, Forward models for nuclear magnetic resonance in carbonate rocks: *The Log Analyst*, vol. 40, no. 4, p. 260–270.
- Toumelin, E., 2002, Monte Carlo simulations of NMR measurements in carbonate rocks under a constant magnetic field gradient: Master's thesis, The University of Texas at Austin.
- Toumelin, E., Torres-Verdín, C., and Chen, S., 2002, Quantification of multi-phase fluid saturations in complex pore geometries from simulations of NMR measurements, SPE-77399, in Annual Technical Conference and Exhibition Proceedings: Society of Petroleum Engineers.
- Zheng, L. H. and Chiew, Y. C., 1989, Computer simulation of diffusion-controlled reactions in dispersions of spherical sinks: *Journal of Chemical Physics*, vol. 90, no. 1, p. 32–327.

ABOUT THE AUTHORS

Emmanuel Toumelin holds an engineering degree from the Ecole Centrale de Lille, France, and an MS in Petroleum Engineering from the University of Texas at Austin. He is now pursuing a PhD degree and is working on micro-scale petrophysics, NMR diffusion, and rock dielectric properties.

Email: toumelin@mail.utexas.edu

Carlos Torres-Verdín received a PhD in Engineering Geoscience from the University of California, Berkeley, in 1991. During 1991-1997, he held the position of Research Scientist with Schlumberger-Doll Research. From 1997-1999, he was Reservoir Specialist and Technology Champion with YPF (Buenos Aires, Argentina). Since 1999, he is an Assistant Professor with the Department of Petroleum and Geosystems Engineering of The University of Texas at Austin, where he conducts research in formation evaluation and integrated reservoir characterization. He has served as Guest Editor for Radio Science, and is currently a member of the Editorial Board of the Journal of Electromagnetic Waves and Applications, and an associate editor for Petrophysics (SPWLA) and the SPE Journal.

Songhua Chen is a staff scientist and project leader for NMR interpretation development at Baker Atlas Houston Technology Center. Prior to joining Baker Atlas, he was a Research Scientist for 5 years with Texas Engineering Experiment Station in College Station, Texas, where he worked in the area of NMR and MRI applications to flow in porous media. Songhua has a BS from Nanjing Institute of Technology in China and a PhD from University of Utah, both in Physics.

D. Marion Fischer is a scientist with Baker Hughes Inteq at Celle, Germany, since December 2001. Prior to joining Inteq, she spent one and half year at Leibniz Institute of Applied Geosciences in Germany as a postdoc doing NMR laboratory research, and a summer at Houston Technology Center of Baker Atlas, USA. Marion received her Diploma (physics) in 1995 and PhD (NMR physics) in 1999, both from the University of Hannover, Germany. Her PhD dissertation topic deals with NMR diffusion measurements in solid-state materials.